Progress In Electromagnetics Research, PIER 54, 245–262, 2005

APPLICATION OF INTEGRAL EQUATION METHOD TO METAL-PLATE LENS STRUCTURES

A. Matsushima, Y. Nakamura, and S. Tomino

Department of Electrical and Computer Engineering
Kumamoto University
Kurokami 2-39-1, Kumamoto 860-8555, Japan

Abstract—The present paper concerns the design, numerical analysis, and measurement for simple metal-plate lens structures. The power of electromagnetic waves can be concentrated by arranging flat strips parallel to one another and adjusting the transverse and longitudinal length of the waveguide regions. The simple designing procedures are described for the lenses with plane, concave, and convex profiles. These steps are practically applied to construct the lenses for the X band. In order to discuss the dependence of focusing properties on the lens and source types, we numerically analyze the scattering problems using the integral equations combined with the moment method. The lenses are made up by aluminum plates, and the field amplitude in the transmission region is measured. We confirm the formation of the focus near the design point.

1. INTRODUCTION

Concentration of the power of electromagnetic waves can be realized by using appropriately shaped dielectric body, natural or artificial, in which the phase velocity is different from that of the free space. One of the means is to take advantage of the property of waveguide modes between parallel metallic plates: the phase is controlled by the transverse and longitudinal length of the guiding regions. The shaping and zoning techniques in such metallic lenses have been developed for several decades [1–3]. This structure was recently attracted attention as an element attached to scanning antennas for anticollision radars [4]. Furthermore the lens may be conveniently used for measuring dielectric constants based on the free space method [5].

In the present paper, we perform the design, numerical analysis, and measurement of metal-plate lens structures. The entire system is theoretically treated as a two-dimensional scattering problem. This simplification is convenient to make metal-plate lenses easily for experimental use unless high efficiency of concentration is required. In the regions between two adjacent plates, only the TE_{10}/TEM mode propagates in the E-/H-wave case for a proper choice of plate spacing. We can design the lens by the condition that the electrical length from the source to the focal point is a constant.

We first describe the simple designing procedures for three kinds of lens profiles, i.e., the plane, concave, and convex ones. Based on this, the examples of practical design in the X band are shown. We next discuss the numerical analysis using the integral equations combined with the moment method. This technique is excellent in view of the accuracy and efficiency in numerical processings, since the edge condition is taken into account in the basis functions and the singularity in kernel functions is extracted and analytically treated. The same scheme was successfully applied for a single curved scatterer [6, 7], a finite number of conducting flat strips on a plane [8], and periodic resistive strip gratings [9]. From the numerical results we discuss the dependence of focusing properties on the lens and source types. Furthermore we make up the lenses by using aluminum plates and measure the field amplitude in the transmission region. The formation of the focus is verified near the design point.

2. STRUCTURE OF METAL-PLATE LENSES

2.1. Formulation of the Problem

As shown in Fig. 1, we place an odd number of metallic plates, numbered as $n = 1, 2, \cdots, N$, in the free space with the permittivity ε_0 and permeability μ_0. The plates are assumed to have infinite conductivity, infinite length along the z axis, and negligible thickness.

Figure 1(a) shows a set of plates having a fixed width w and unequal spacings. The contour in the xy plane is expressed by $|x| \leq w/2,\ y = b_n$. Figure 1(b) is a set of plates having a fixed spacing s and unequal widths. The contour is written as $-w/2 - p_{0n} \leq x \leq$

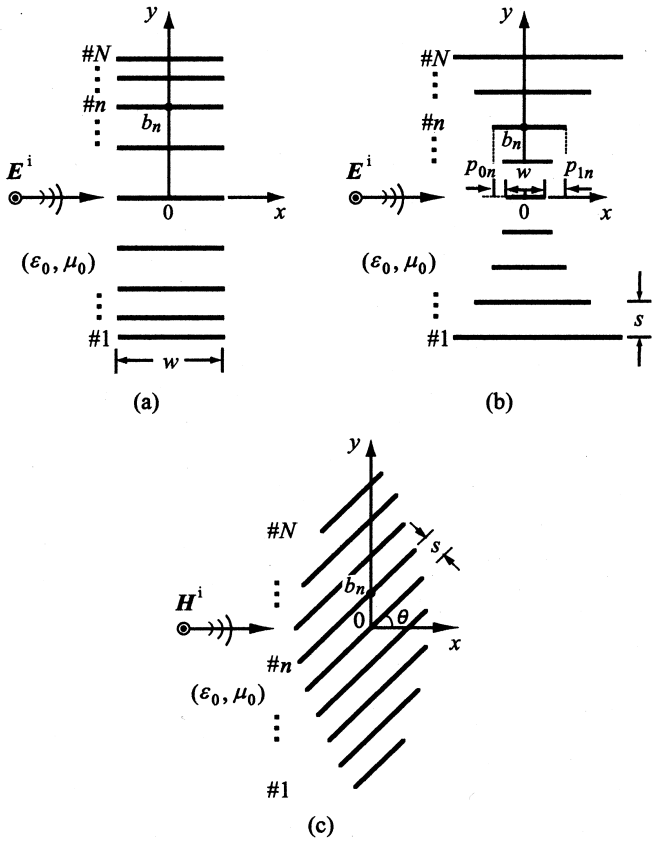

Figure 1. Geometry of the problem. (a) Plane type for E-wave with fixed width w. (b) Concave type for E-wave with fixed spacing s. (c) Convex type for H-wave with fixed spacing s.

$w/2 + p_{1n}$, $y = b_n \equiv (2n - N - 1)s/2$, where p_{0n} and p_{1n} are the increments in the $-x$ and $+x$ sides, respectively, with regard to the width of central plate w. Besides in Fig. 1(c), the plates having unequal width are allocated with the spacing s and inclined angle θ with respect to the x axis. They cross the y axis at $y = b_n \equiv (2n-N-1)s/(2\cos\theta)$. Let us call these three sets, in accordance with the outlines, the plane, concave, and convex types.

We consider the two-dimensional problem of the E- and H-waves, where the respective electric and magnetic fields have only the z component. The structures of Fig. 1(a), (b) work as electromagnetic wave lenses for E-wave, and so does Fig. 1(c) for H-wave. Representing E_z or H_z by the letter u, we have the relation $u^{\mathrm{t}}(P) = u^{\mathrm{i}}(P) + u^{\mathrm{s}}(P)$, where the superscripts i, s, t denote the incident, scattered, and total fields, respectively. Here, P is an observation point (x, y), and the time factor $\exp(j\omega t) = \exp(j2\pi ft)$ is omitted throughout.

Let the incident field be a cylindrical wave emerged from a line source placed at the point $S(-r_0, 0)$ $(r_0 > 0)$. It is written as

$$u^{\mathrm{i}}(P) = \Phi^{\mathrm{i}}(P)\,\frac{\exp(-jk|SP|)}{\sqrt{k|SP|}} \tag{1}$$

where $|SP| = \sqrt{(x + r_0)^2 + y^2}$ is the distance, $k = \omega\sqrt{\varepsilon_0\mu_0}$ is the wavenumber, and $\lambda = 2\pi/k$ is the wavelength in the free space. The normalized radiation pattern function is given as follows [10].

- Isotropic, i.e., $\Phi^{\mathrm{i}}(P) = 1$.
- Pattern for H-plane horn (E-wave), i.e., $\Phi^{\mathrm{i}}(P) = \cos\eta/[1 - (2\eta/\pi)^2]$. Here, $\eta = (\pi a/\lambda)\cdot(y/|SP|)$ with a being the aperture width of a horn.
- Pattern for E-plane horn (H-wave), i.e., $\Phi^{\mathrm{i}}(P) = \sin\eta/\eta$, where η was defined previously.

2.2. Design of Lenses

2.2.1. Refractive Index and Velocity

In the case of E-wave, only the TE_{10} mode can propagate in the parallel plate waveguide regions if $\lambda/2 < s < \lambda$. The phase velocity of this mode is the same as that in the medium with the refractive index $\nu = \sqrt{1 - [\lambda/(2s)]^2}$ (< 1) and is greater than that of the free space [11]. Therefore we can concentrate the fields by decreasing s or increasing w with the distance from the x axis.

On the other hand, in the H-wave case, only the TEM mode can propagate if $s < \lambda/2$. Because its phase velocity is the same as that in

the free space, the inclination of the plates makes the velocity smaller in the x direction. The metal set is thereby regarded as an equivalent medium with the refractive index $\nu = 1/\cos\theta$ (> 1), so that we can apply the same principle as conventional dielectric lenses.

Figure 2 shows the principle of focusing, where AL/AR denotes the contour of waveguide apertures in the left/right hand side, and the focal point F is located at $(r_1, 0)$. In designing lenses, we disregard the shift of phase reference at the aperture terminals [12] and the multiple reflections of the waveguide modes.

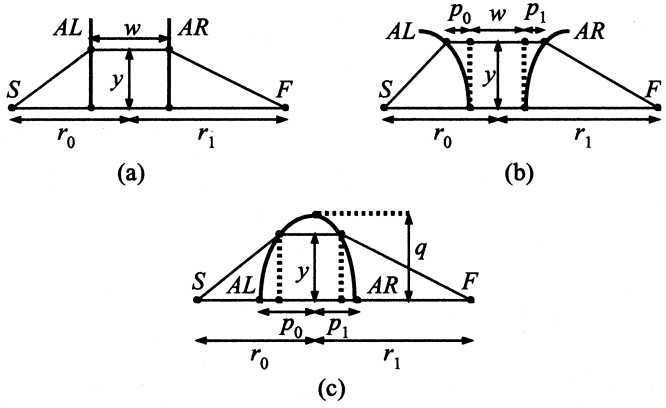

Figure 2. Principle of focusing. (a) Plane type. (b) Concave type. (c) Convex type.

2.2.2. Plane Type Lens for E-wave

Although the refractive index ν is a discrete value determined by each spacing s, we tentatively regard it as a continuous function of y. Referring to Fig. 2(a), we have the condition that the electrical length from S to F is independent of the path:

$$r_0 + r_1 + [\nu(0) - 1]w = \sqrt{(r_0^2 - w/2) + y^2} + \sqrt{(r_1^2 - w/2) + y^2} + \nu(y)w \quad (1)$$

This leads

$$\nu(y) = \nu(0) - 1 - \frac{1}{w}\left[\sqrt{\left(r_0^2 - \frac{w}{2}\right) + y^2} + \sqrt{\left(r_1^2 - \frac{w}{2}\right) + y^2} - r_0 - r_1\right] \quad (2)$$

In order to facilitate the coupling between the free space and waveguides, we fix $s(0)$ at its maximum λ and substitute the corresponding value $\nu(0) = \sqrt{3}/2$ into the right hand side of (3). We then draw the monotonically decreasing curve with the abscissa and ordinate being y and $s(y) = (\lambda/2)/\sqrt{1-[\nu(y)]^2}$ (Equation (3) is used for $\nu(y)$), respectively. The positions b_n are determined by applying the step approximation to the above curve. The following steps are convenient.

1: Put the central plate at $y = 0$.

2: Once b_{n-1} is determined, the position of the nearest upper plate is given by $b_n = b_{n-1} + s(b_{n-1})$. However this formula yields the step approximation curve always upper than that of $s(y)$. Such errors are reduced by the iterative computation using $b_n = b_{n-1} + s(b_{n-1} + s(b_{n-1})/2)$ instead of the above formula.

3: Repeat Step **2** while $\nu(y) > 0$.

4: Arrange the plates symmetrically in the region $y < 0$.

According to these steps, the lens named ML1 is designed at $f = 10.525\,\text{GHz}$, $\lambda = 28.5\,\text{mm}$, $w = 100\,\text{mm}$, $r_0 = r_1 = 350\,\text{mm}$. The number of plates N is 19, and their position, from b_{19} to b_{10}, is (in millimeters)

$$\left\{ \begin{array}{ccccc} 168.1 & 153.8 & 139.3 & 124.3 & 108.6 \\ 91.7 & 73.1 & 52.1 & 27.8 & 0.0 \end{array} \right\} \qquad \text{(ML1)}$$

The maximum of spacing $b_{11} - b_{10} = 27.8\,\text{mm}$ is a little less than λ, whereas the minimum $b_{19} - b_{18} = 14.3\,\text{mm}$ is slightly greater than $\lambda/2$.

2.2.3. Concave Type Lens for E-wave

Since the refractive index ν is fixed, the condition of constant electrical length in Fig. 2(b) is

$$r_j - \frac{w}{2} = \sqrt{\left(r_j - \frac{w}{2} - p_j\right)^2 + y^2} + p_j\nu \quad (j = 0, 1) \qquad (4)$$

This leads the design formula for the increment

$$p_j = \frac{r_j - w/2}{1+\nu}\left[1 - \sqrt{1 - \frac{1+\nu}{1-\nu}\left(\frac{y}{r_j - w/2}\right)^2}\right] \qquad (5)$$

The lens structure becomes symmetrical if $r_0 = r_1$.

Based on the above, the lens named ML2 is designed at $f = 10.525\,\text{GHz}$, $\lambda = 28.5\,\text{mm}$, $s = 18.5\,\text{mm}$, $\nu = 0.638$, the guide

wavelength $\lambda_g = \lambda/\nu = 44.6\,\text{mm}$, $r_0 = r_1 = 300\,\text{mm} + w/2$. The number of plates N is 15, and the increment, from p_{j1} to p_{j8} is (in millimeters)

$$\{\ 110.7 \quad 70.2 \quad 44.9 \quad 27.3 \quad 14.8 \quad 6.4 \quad 1.6 \quad 0.0\ \} \qquad \text{(ML2)}$$

It is enough to choose the minimum width $w \approx 2\lambda_g$ so that the waveguide mode may be formed. Here we set $w = 100\,\text{mm}$.

2.2.4. Convex Type Lens for H-wave

In Fig. 2(c), the lens profile is given by the hyperbola

$$\frac{\left(x + \dfrac{r_0 + \nu p_0}{\nu + 1}\right)^2}{\left(\dfrac{r_0 - p_0}{\nu + 1}\right)^2} - \frac{y^2}{\dfrac{\nu - 1}{\nu + 1}(r_0 - p_0)^2} = 1 \qquad (6)$$

for $-p_0 < x < 0$ (AL), whereas for $0 < x < p_1$ (AR) the symbols r_0 and p_0 are replaced with $-r_1$ and $-p_1$, respectively. We first set the spacing s, the refractive index ν, and the transverse size q, and then go through the following steps.

1: Compute p_0 and p_1 by $p_i = (\sqrt{r_i^2 + q^2} - r_i)/(\nu - 1)$.

2: Determine $y = b_1, b_2, \cdots, b_N$ within the interval $-q < y < q$.

3: Obtain the edge position of the plates as an intersection of the line $y = x\sqrt{\nu^2 - 1} + b_n$ and (6). For example, the x coordinate of the left side edge is

$$x_n^{(0)} = -\frac{1}{2} \cdot \frac{[2r_0 + (\nu - 1)p_0]\, p_0 - \dfrac{b_n^2}{\nu - 1}}{r_0 + \nu p_0 - \sqrt{\dfrac{\nu + 1}{\nu - 1}}\, b_n} \qquad (7)$$

For the right side edge we follow the same replacement as was stated just after (6). From these values we can also get the y coordinate of the edges and the plate widths.

According to these steps, the lens named ML3 is designed at $f = 10.525$ GHz, $\lambda = 28.5\,\text{mm}$, $s = 10.0\,\text{mm}$, $\nu = 1.743$, $\theta = 55°$, $q = 130\,\text{mm}$, $p_0 = p_1 = 31.4\,\text{mm}$, $r_0 = r_1 = 350\,\text{mm}$. The number of plates N is 15, and the x coordinate of the left edge, from $x_1^{(0)}$ to $x_{15}^{(0)}$,

and the width, from w_1 to w_{15}, are (in millimeters)

$$\left\{\begin{array}{cccccccc} -2.1 & -6.6 & -10.9 & -15.0 & -18.9 & -22.4 & -25.5 & -28.1 \\ -30.1 & -31.2 & -31.3 & -29.9 & -26.4 & -19.7 & -7.9 & \end{array}\right\}$$
$$\left\{\begin{array}{cccccccc} 17.5 & 45.8 & 65.0 & 78.3 & 87.4 & 93.4 & 96.8 & 97.9 \\ 96.8 & 93.4 & 87.4 & 78.3 & 65.0 & 45.8 & 17.5 & \end{array}\right\} \tag{ML3}$$

3. INTEGRAL EQUATION ANALYSIS

3.1. E-Wave Case

Let us express the contour of the metallic plates in the xy-plane by $C = \sum_{n=1}^{N} C_n$ and specify a point on C_n by $(x_n^{(0)} + (t/k)\cos\theta_n, y_n^{(0)} + (t/k)\sin\theta_n)$. Here, the parameter $t = k\sqrt{(x - x_n^{(0)})^2 + (y - y_n^{(0)})^2}$ $(0 \le t \le kw_n)$ is an electrical length from one edge to an observation point, and θ_n is an inclined angle with respect to the x axis.

The integral equation is written as

$$\int_C G(P,Q) f(Q)\, dt_Q = g(P) \quad (P \in C) \tag{8}$$

where

$$\left\{\begin{array}{l} G(P,Q) = (4j)^{-1} H_0^{(2)}(k|PQ|) \\ f(Q) = -jZK_z(Q), \quad g(P) = -u^{\mathrm{i}}(P) \end{array}\right. \tag{9}$$

In the above definition, $H_0^{(2)}$ is the zero order Hankel function of the second kind, $Z = \sqrt{\mu_0/\varepsilon_0}$ is the intrinsic impedance, and K_z is the current density induced on the plates. Using the solution of (8), we can express the scattered field $u^{\mathrm{s}}(P) = E_z^{\mathrm{s}}(P)$ by

$$u^{\mathrm{s}}(P) = \int_C G(P,Q) f(Q)\, dt_Q \quad (P \notin C) \tag{10}$$

Let us solve (8) by the moment method. First the unknown function is approximated as

$$f(Q) \approx \sum_{l=0}^{L_n} f_{nl}\, \tau_{nl}(Q) \quad (Q \in C_n;\ n = 1, 2, \cdots, N) \tag{11}$$

where the basis function is chosen, by taking account of the edge condition [14], as

$$\tau_{nl}(t) = \frac{T_l\left(\dfrac{2t}{kw_n} - 1\right)}{\sqrt{t(kw_n - t)}} \quad (n = 1, 2, \cdots, N;\ l = 0, 1, \cdots, L_n) \tag{12}$$

with T_l being the l-th order Chebyshev polynomial of the first kind. We next substitute (11) into (8), multiply both sides by the testing functions (defined on $P \in C_{n'}$)

$$\sigma_{n'l'}(t) = T_{l'}\left(\frac{2t}{kw_{n'}} - 1\right) \quad (n' = 1, 2, \cdots, N;\ l' = 0, 1, \cdots, L_n) \tag{13}$$

and integrate over C. The above procedure leads us to the simultaneous linear equations

$$\sum_{n=1}^{N}\sum_{l=0}^{L_n} \alpha_{n'l',nl}\, f_{nl} = \beta_{n'l'} \quad (n' = 1, 2, \cdots, N;\ l = 0, 1, \cdots, L_n) \tag{14}$$

where

$$\begin{cases} \alpha_{n'l',nl} = \displaystyle\int_{C_{n'}} u_{nl}(P)\, \sigma_{n'l'}(P)\, dt_P \\ \beta_{n'l'} = \displaystyle\int_{C_{n'}} g(P)\, \sigma_{n'l'}(P)\, dt_P \\ u_{nl}(P) = \displaystyle\int_{C_n} G(P,Q)\, \tau_{nl}(Q)\, dt_Q \end{cases} \tag{15}$$

The coefficients $\alpha_{n'l',nl}$ and $\beta_{n'l'}$ are evaluated by the conventional quadrature formulas such as midpoint rule. For the function $u_{nl}(P)$ we apply the Gauss-Chebyshev rule [13] by taking into account the behavior of τ_{nl} near the edges. In particular, if the point P is included in the contour C_n, we extract the singularity of Hankel function as

$$\begin{aligned} u_{nl}(P_0) = &-\frac{1}{2\pi}\int_0^{kw_n} \log|t_0 - t|\, \tau_{nl}(t)\, dt \\ &+ \frac{1}{4j}\int_0^{kw_n}\left[H_0^{(2)}(|t_0 - t|) - \frac{2}{j\pi}\log|t_0 - t|\right]\tau_{nl}(t)\, dt \end{aligned} \tag{16}$$

and then evaluate the first and second terms analytically and numerically, respectively. Here, t_0 is the electrical length from one edge to P_0 along C_n.

3.2. H-Wave Case

The integro-differential equation is

$$\left(\frac{d^2}{dt_P^2} + 1\right)\int_C G(P,Q) f(Q)\, dt_Q = g(P) \quad (P \in C) \tag{17}$$

where $G(P,Q)$ is the same as in (9), and the other functions are

$$f(Q) = -jK_t(Q), \quad g(P) = \frac{j}{k}\,\hat{\nu}_P \cdot \nabla_P u_z^{\mathrm{i}}(P) \tag{18}$$

with the current density K_t, the unit normal vector $\hat{\nu}_P = (-\sin\theta_n, \cos\theta_n)$ $(P \in C_n)$, and the two-dimensional differential operator ∇_P. The use of the solution of (17) yields the scattered field $u^{\mathrm{s}}(P) = H_z^{\mathrm{s}}(P)$ as

$$u(P) = \frac{j}{k} \int_C \hat{\nu}_Q \cdot \nabla_Q G(P,Q) f(Q)\, dt_Q \quad (P \notin C) \tag{19}$$

In the context of the moment method, the unknown function is approximated in the form of (11). However the basis is changed into

$$\tau_{nl}(t) = \sqrt{t(kw_n - t)}\, U_l\left(\frac{2t}{kw_n} - 1\right) \tag{20}$$

where U_l is the l-th order Chebyshev polynomial of the second kind. The testing function is given by (13) with $T_{l'}$ replaced by $U_{l'}$. The simultaneous linear equations are again expressed as (14), (15). Paying attention to the order of singularity of the kernel function, we decompose as

$$\begin{aligned} u_{nl}(P_0) = {} & \frac{1}{2\pi} \int_0^{kw_n} \frac{\tau_{nl}(t)}{(t_0 - t)^2}\, dt \\ & - \frac{1}{4\pi} \int_0^{kw_n} \log|t_0 - t|\, \tau_{nl}(t)\, dt \\ & + \frac{1}{4j} \int_0^{kw_n} \left[\frac{H_1^{(2)}(|t_0 - t|)}{|t_0 - t|} - \frac{2j}{\pi(t_0 - t)^2} - \frac{1}{j\pi} \log|t_0 - t| \right] \tau_{nl}(t)\, dt \end{aligned} \tag{21}$$

The first and second terms in the right hand side above can be evaluated analytically, and the third term is treated numerically.

4. NUMERICAL RESULTS

By the numerical experiment, we found that it is enough to set the truncation number L_n in (11) as about $5(w_n/\lambda + 1)$, with the number of division in the quadrature in (15) being $3(L_n + 1)$. The norm error, which is defined by the norm of the difference between both sides of (8), (17) normalized by that of $g(P)$, is always less than 0.2 %. The error on the optical theorem at plane wave incidence is the same degree as or less than the norm error.

Figures 3, 4, and 5 show the near fields for the nominated lenses ML1, ML2, and ML3, respectively, where the value is normalized by the incident amplitude at the center of each lens. As described in **2.1**, two kinds of sources, isotropic and beam, are treated. The aperture of the horn a is 94 mm and 70 mm in the H- and E-planes, respectively.

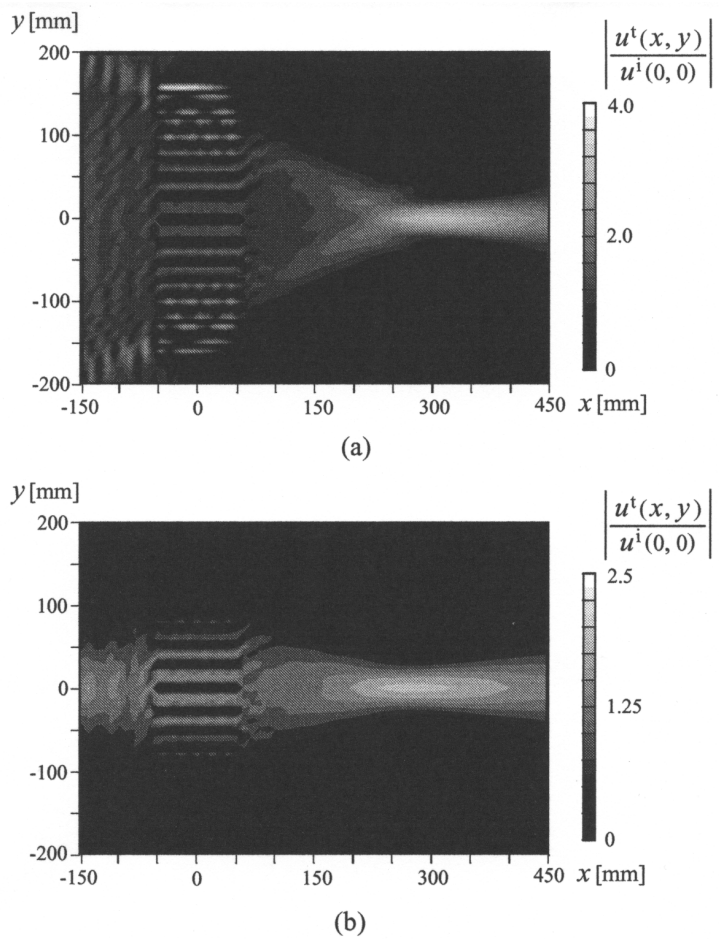

Figure 3. Normalized electric field amplitude around the plane type lens ML1. (a) Isotropic source. (b) Beam source.

These yield the first null at ± 25 and ± 17 degrees. That is, little of the incident wave enters the several waveguides in the outer parts the lenses. On the other hand, for the isotropic source, all the waveguides contribute to the formation of focus, so that the field strength therein becomes about 2 times compared to the case of beam source. The focal point for beam incidence is at $x = 270$, 310, and 290 mm for the respective figures, which is by 10–20% less than the designed value 350 mm. This is due to the assumption stated in the last few lines of 2.2.1. Interestingly, the field in Fig. 5 is guided to the upper right

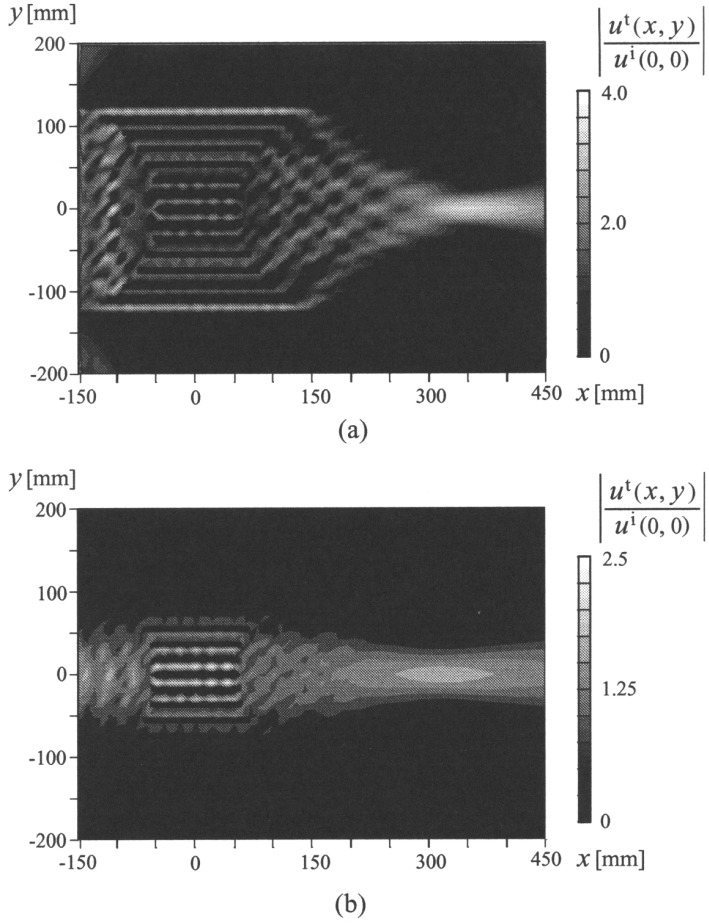

Figure 4. Normalized electric field amplitude around the concave type lens ML2. (a) Isotropic source. (b) Beam source.

apertures and distributed unsymmetrically in the transmission region, but is concentrated around the x axis.

We confirmed that the equiphase lines are almost parallel to each other within the $3\lambda \times 3\lambda$ square region surrounding the focus, although figures are omitted here. In addition, these lines are nearly perpendicular to the equiamplitude ones. That is, the equiphase lines for the lenses ML1 and ML2 are parallel to the y axis, while for ML3 they slant by about 10 degrees clockwise with respect to the y axis.

Figure 6 shows the field amplitude on the lens axis at beam

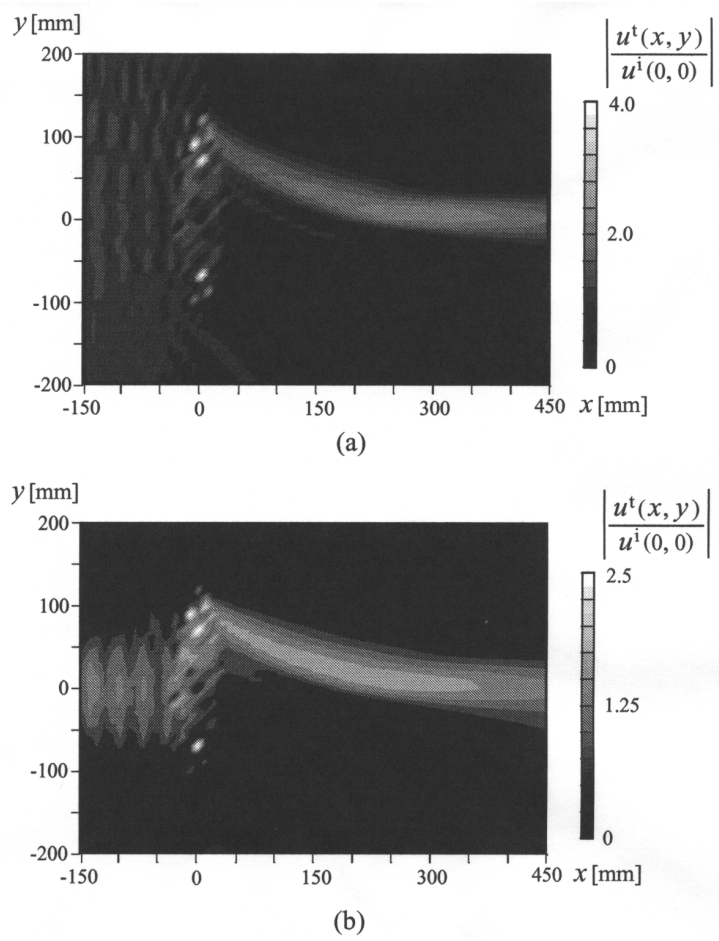

Figure 5. Normalized magnetic field amplitude around the convex type lens ML3. (a) Isotropic source. (b) Beam source.

incidence for different size and arrangement of the plates. The solid lines correspond to the lenses ML1, ML2, and ML3, to which the measured values are attached by filled circles. Here, the lenses were made up by long rectangular aluminum plates and the experiment was carried out in a simple anechoic chamber. Taking into account that the experimental setup includes a pyramidal horn as an excitation and thereby constitutes a three dimensional system, we compensate the measured values by multiplying the factor $\sqrt{(r_0 + x)/r_0}$. Although the agreement between the theoretical and experimental results is

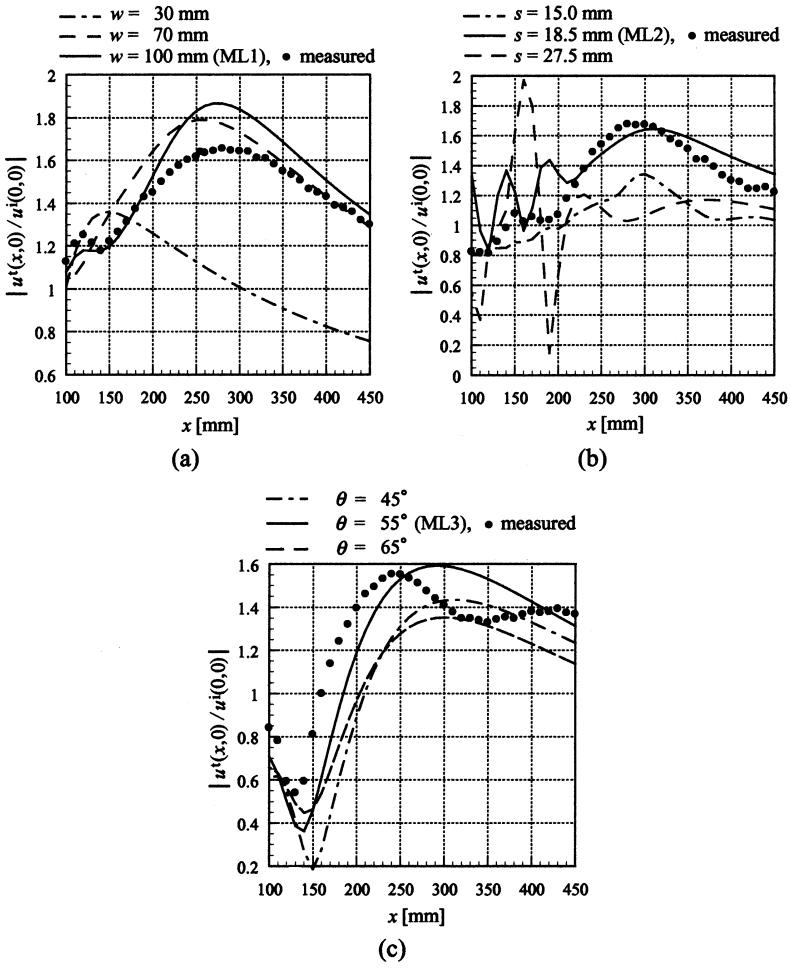

Figure 6. Normalized field amplitude on the lens axis with beam excitation and $r_0 = r_1 = 350\,\text{mm}$. (a) Plane type. (b) Concave type. (c) Convex type.

not complete because of nonidentical systems, the latter exhibits the formation of focus relatively well. The other curves are drawn by changing one of the parameters and repeating the design and computation. The nominated lenses ML1, ML2, and ML3 have the highest ability of concentration among all.

It is of interest to observe the stability with the variation of frequency, since the broad band characteristic is important in pulse

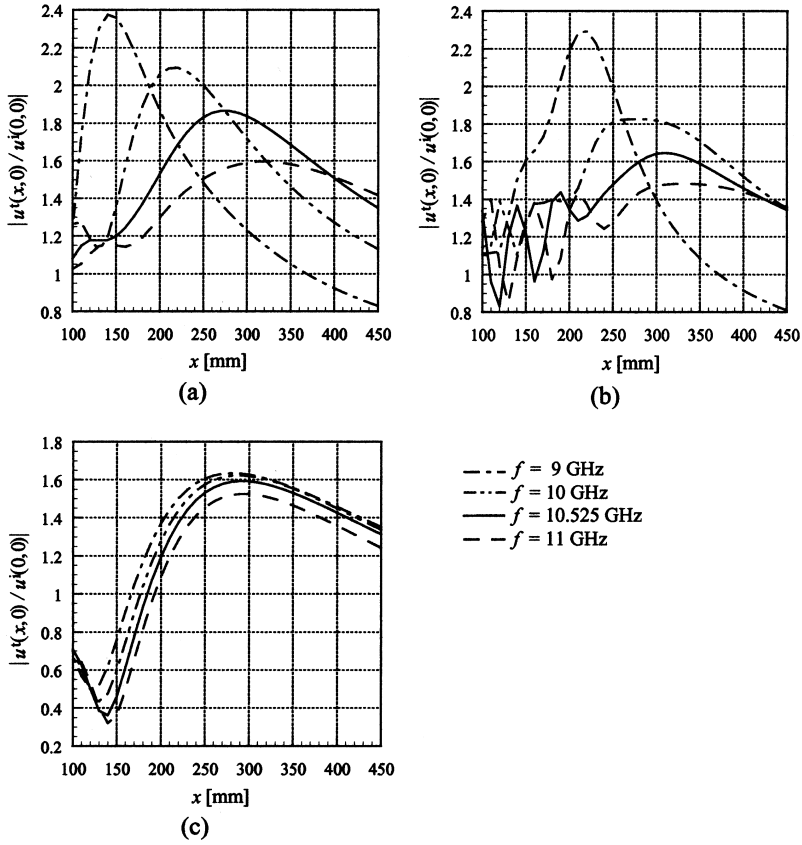

Figure 7. Normalized field amplitude on the lens axis with beam excitation and $r_0 = r_1 = 350\,\text{mm}$. (a) Plane type ML1. (b) Concave type ML2. (c) Convex type ML3.

wave transmission. This is shown in Fig. 7 for the lenses ML1, ML2, and ML3. As the lenses are designed at the fixed value $f = 10.525\,\text{GHz}$, the field may not be concentrated near $x = 350\,\text{mm}$ for other frequencies. For the lenses ML1 and ML2, the focal point moves toward the incident side and the peak value increases as the frequency decreases. This is due to the fact that the phase velocity in the waveguide region is large for low frequencies. Nevertheless we see a small amount of shift in the four curves for ML3, because the refractive index for the convex type lens is independent of the frequency.

5. CONCLUSIONS

We have performed the design, numerical analysis, and measurement for three types of metal-plate lenses. The focusing properties are discussed by the numerical results based on the integral equations and the moment method. By experiments we confirm that the focus is made up near the design point. The adopted structures are simple but may be useful in the experiment on electromagnetic wave scatterings or the measurement of dielectric constants.

It is well known that some additional phase shift occurs at the interface between the parallel plates and free space. Closer coincidence between numerical and experimental results might be expected if the phase shifts found for infinite arrays of parallel plates [15] was incorporated. This is one of our future problems.

The present paper treated the simplified two dimensional problems as a starting point. However the practical lenses are mainly composed of not rectangular but concave shaped metallic plates. This aims at the improvement of the degree of concentration by forming focuses in both E- and H-planes simultaneously. Another attempt is to promote the coupling between the free space and waveguides by inserting matching diaphragm inside the guides. These subjects deserve further attentions.

ACKNOWLEDGMENT

The authors thank Mr. Takashi Iki, the student of Kumamoto University, for his assistance in experiments. This work was supported in part by the Grants-in-Aid for Scientific Research, Japan Society for the Promotion of Science (C)(2)(15560299).

REFERENCES

1. Silver, S., *Microwave Antenna Theory and Design*, McGraw-Hill, New York, Chap. 11, 1949.
2. Collin, R. E. and F. J. Zucker, *Antenna Theory*, Part 2, Chap. 18, McGraw-Hill, New York, 1969.
3. Johnson, R. C., *Antenna Engineering Handbook*, Third Edition, Sec. 18.3, McGraw-Hill, New York, 1993.
4. Gallée, F., G. Landrac, and M. M. Ney, "Artificial lens for third-generation automotive radar antenna at millimetre-wave frequencies," *IEE Proceedings–Microwave, Antennas Propagat.*, Vol. 150, No. 6, 470–476, 2003.

5. Ghodgaonkar, D. K., V. V. Varadan, and V. K. Varadan, "A free-space method for measurement of dielectric constants and loss tangent at microwave frequencies," *IEEE Trans. Instrum. Meas.*, Vol. 38, No. 3, 789–793, 1989.
6. Frenkel, A., "External modes of two-dimensional thin scatterers," *IEE Proceedings*, Part H, Vol. 130, No. 3, 209–214, 1983.
7. Panasyuk, B. B., M. P. Savruk, and Z. T. Nazarchuk, *Method of Singular Integral Equations in Two-Dimensional Diffraction Problems*, Naukova Dumka, Kiev, 1985 (in Russian).
8. Matsushima, A. and T. Itakura, "Singular integral equation approach to electromagnetic scattering from a finite periodic array of conducting strips," *J. Electromagn. Waves Applic.*, Vol. 5, No. 6, 545–562, 1991.
9. Matsushima, A., T. L. Zinenko, H. Minami, and Y. Okuno, "Integral equation analysis of plane wave scattering from multilayered strip gratings," *J. Electromagn. Waves Applic.*, Vol. 12, No. 11, 1449–1469, 1998.
10. Collin, R. E., *Antennas and Radiowave Propagation*, Sec. 4.4, McGraw-Hill, New York, 1985.
11. Pozar, D. M., *Microwave Engineering*, Sec. 3.3, John Wiley & Sons, New York, 1998.
12. Marcuvitz, N., *Waveguide Handbook*, Sec. 5.23, McGraw-Hill, New York, 1951.
13. Abramowitz, M. and I. A. Stegun (eds.), *Handbook of Mathematical Functions*, 889, Dover, New York, 1972.
14. Meixner, J., "The behavior of electromagnetic fields at edges," *IEEE Trans. Antennas Propagat.*, Vol. AP-20, No. 4, 442–446, 1972.
15. Collin, R. E., *Field Theory of Guided Waves*, Second edition, Chaps. 10 and 12, IEEE Press, New York, 1991.

Akira Matsushima was born in Kumamoto, Japan, in 1958. He received the B.E. degree from Kumamoto University, Kumamoto, Japan, in 1980, and the M.E. and D.E. degrees from Kyushu University, Fukuoka, Japan, in 1982 and 1994, respectively. He joined the Department of Electrical and Computer Engineering, Kumamoto University, in 1982 as a Research Associate, where he is now an Associate Professor. He is currently working in the area of numerical methods for electromagnetic boundary value problems and microwave transmission lines. Dr. Matsushima is a member of the Institute of

Electrical Engineers (IEE) of Japan, and the Institute of Electronics, Information and Communication Engineers (IEICE) of Japan.

Yumi Nakamura was born in Kumamoto, Japan, in 1980. She received the B.E. degree from Kumamoto University, Kumamoto, Japan, in 2003. She is currently working toward the M.E. degree in the same university. Her research interests include electromagnetic scattering problems. Ms. Nakamura is a student member of the Institute of Electronics, Information and Communication Engineers (IEICE) of Japan.

Satoshi Tomino was born in Kumamoto, Japan, in 1981. He received the B.E. degree from Kumamoto University, Kumamoto, Japan, in 2004. He is currently working toward the M.E. degree in the same university. His research interests include electromagnetic scattering problems. Mr. Tomino is a student member of the Institute of Electronics, Information and Communication Engineers (IEICE) of Japan.